

On the flutter characteristics of separated two box girders

Masaru Matsumoto[†], Rikuma Shijo[‡], Akitoshi Eguchi[‡], Tetsuya Hikida[‡],
Hitoshi Tamaki[‡] and Keisuke Mizuno^{‡†}

*Department of Civil and Earth Resources Engineering, Kyoto University,
Yoshida Hon-machi, Sakyo-ku, Kyoto, Japan*

(Received January 31, 2004, Accepted May 2, 2004)

Abstract. The flutter characteristics of long span bridges are discussed from the point of the unsteady pressure distribution on bridge deck surface during heaving/torsional vibration related to the aerodynamic derivatives. In particular, it is explained that the coupling terms, which consist of A_1^* and H_3^* , play a substantial role on the coupled flutter, in comparison with the flutter characteristics of various structural sections. Also the effect of the torsional/heaving frequency ratio of bridge structures on the flutter instability is discussed from the point of the coupling effect between heaving and torsional vibrations.

Keywords: flutter stabilization; a super-long span bridge; A_1^* or/and H_3^* control; unsteady pressure characteristics; two-separate box girders with a vertical plate.

1. Introduction

How to stabilize the flutter instability has been a substantial design-issue of a long span bridge since Tacoma Narrows Bridge failure in 1940. However, since a bridge girder, in general, does not have a stream-line section but so called bluff section, whose flutter characteristics become worse than the ones of a thin plate or an airfoil, and moreover, the flutter stability performance of a super-long span bridge is required to be much better than the one of thin plate even though with the same structural dynamics, the safe design of a super-long span bridge against the flutter instability can be said to be an extremely difficult issue. The girder sections of Akashi Strait Bridge ($l=1991$ m, l = main span length) and Messina Strait Bridge ($l=3300$ m, abbreviated by MSB hereafter), which can be aerodynamically stabilized by a truss-stiffened girder with the grating-parts and a central vertical plate, and the three box girders with the air-gaps in between and with the flap-plates and the wind shelters at the girder-edges, respectively, have been researched through a lot of tried-and-error wind tunnel tests. In order to develop more reasonable design of a super long span bridge, mechanism of the flutter instability should be more clearly clarified in relation to the flow control around a bridge girder, the unsteady pressure characteristics related to flutter instability and the role of aerodynamic derivatives. The authors have pointed out importance of the control of A_1^* or/and H_3^* for the coupled flutter stabilization by use of the "Step-by-Step" flutter analysis, which is hereafter abbreviated in SBSFA, for both torsional and heaving branch (Matsumoto, *et al.* 1994). Recently, it

[†] Professor

[‡] Graduate Student

^{‡†} Student

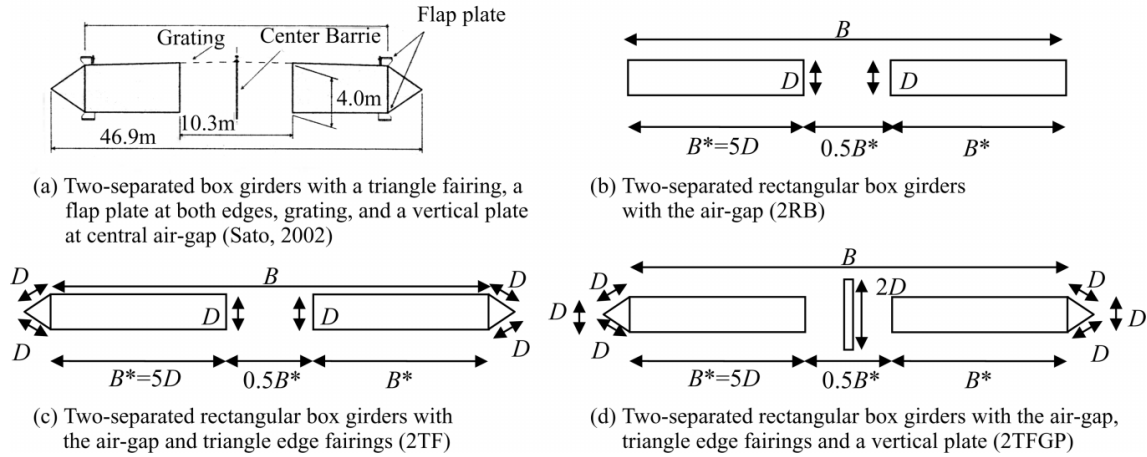


Fig. 1 Various kinds of two-separated box girders for long-span bridge

has been reported that the two separate-box girders with a triangle fairing and a flap-plate at both edges and a vertical plate at the central air-gap, as shown in Fig. 1(a), indicates extremely stable property against the flutter instability (Sato, *et al.* 2002), but the stabilizing mechanism is not clarified. Therefore, in this study, basing upon the unsteady pressure and the aerodynamic derivatives, the flutter characteristics of a similar section are investigated in comparison with the other bridge girders, and the key-points for the flutter stabilization of the “separated” sections are pointed out.

2. Wind tunnel tests

The wind tunnel used in this study has 1.8 m height and 1.0 m width. The models, mainly discussed here, are three different type of two-separated box girders with the air-gap width of $0.5B^*$ ($B^*=100$ mm: chord length of each box section), those are two-separated rectangular girders, each with $B^*/D=5$ ($D=20$ mm: girder height), additionally with-triangle edge fairing, and besides with-a vertical plate (so-called “gap-plate”), with $2D$ height and $B^*/30$ width installed in a central air-gap part as illustrated in Fig. 1(b),(c),(d). And 19 pressure taps are set with equal interval on each box section. Those models are expressed by the symbols of 2RB, 2TF and 2TFGP, hereafter respectively. The unsteady pressures are measured under the forced heaving or torsional vibration and the unsteady lift and pitching moment are directly measured as well. And frequency of forced heaving or torsional vibration is 1.3 Hz. The measurements have been mainly carried out under the conditions of the angle of attack α of 0° and in smooth flow, but some additional cases under $\alpha=3^\circ$ and 5° and in turbulent flow generated by a grid with the intensity of 5%. Therefore, if no particular explanation of test condition, it corresponds to that of $\alpha=0^\circ$ and in smooth flow.

3. The unsteady pressure characteristics and the aerodynamic derivatives

The flow field around heaving or torsional steady vibrating body produces the specified unsteady pressure on vibration body surface in synchronization. Therefore, the unsteady forces caused by

vibration are obtained from the integration of the unsteady pressures, taking into account the pressure amplitude and the phase-lag between the pressure and the girder vibration. The unsteady lift and pitching moment in the heaving and torsional 2DOF system are expressed by eight aerodynamic derivatives, H_i^* and A_i^* ($i=1-4$), proposed by Scanlan, *et al.* (1974), are expressed as follows:

$$L = \frac{1}{2}\rho(2b)V^2 \left\{ kH_1^* \frac{\dot{\eta}}{V} + kH_2^* \frac{b\dot{\phi}}{V} + k^2 H_3^* \phi + k^2 H_4^* \frac{\eta}{b} \right\} \quad (1)$$

$$M = \frac{1}{2}\rho(2b^2)V^2 \left\{ kA_1^* \frac{\dot{\eta}}{V} + kA_2^* \frac{b\dot{\phi}}{V} + k^2 A_3^* \phi + k^2 A_4^* \frac{\eta}{b} \right\} \quad (2)$$

where, L/M =unsteady lift force/pitching moment per unit length, η/ϕ =heaving/torsional displacement (downward/nose-up positive), V =wind velocity, ρ =air density, b =half chord length, $k=b\omega/V$ =reduced frequency, ω =flutter circular frequency. These aerodynamic derivatives are related with the unsteady pressure properties, which are obtained from the forced-heaving or torsional vibration with steady amplitude, as follows (Matsumoto, *et al.* 1997):

$$\begin{aligned} H_1^* &= \frac{-V^2}{2b\omega^2\eta_0} \int_{-1}^1 \tilde{C}_p \cos \Psi_H dx = \frac{V^2}{2b\omega^2\eta_0} \int_{-1}^1 \tilde{C}_{pH_1^*} dx, \\ H_2^* &= \frac{V^2}{2b^2\omega^2\phi_0} \int_{-1}^1 \tilde{C}_p \sin \Psi_T dx = \frac{V^2}{2b^2\omega^2\eta_0} \int_{-1}^1 \tilde{C}_{pH_2^*} dx, \\ H_3^* &= \frac{-V^2}{2b^2\omega^2\phi_0} \int_{-1}^1 \tilde{C}_p \cos \Psi_T dx = \frac{V^2}{2b^2\omega^2\eta_0} \int_{-1}^1 \tilde{C}_{pH_3^*} dx, \\ H_4^* &= \frac{-V^2}{2b\omega^2\eta_0} \int_{-1}^1 \tilde{C}_p \sin \Psi_H dx = \frac{V^2}{2b\omega^2\eta_0} \int_{-1}^1 \tilde{C}_{pH_4^*} dx, \\ A_1^* &= \frac{-V^2}{2b\omega^2\eta_0} \int_{-1}^1 \tilde{C}_p x \cos \Psi_H dx = \frac{V^2}{2b\omega^2\eta_0} \int_{-1}^1 \tilde{C}_{pA_1^*} dx, \\ A_2^* &= \frac{V^2}{2b^2\omega^2\phi_0} \int_{-1}^1 \tilde{C}_p x \sin \Psi_T dx = \frac{V^2}{2b^2\omega^2\eta_0} \int_{-1}^1 \tilde{C}_{pA_2^*} dx, \\ A_3^* &= \frac{-V^2}{2b^2\omega^2\phi_0} \int_{-1}^1 \tilde{C}_p x \cos \Psi_T dx = \frac{V^2}{2b^2\omega^2\eta_0} \int_{-1}^1 \tilde{C}_{pA_3^*} dx, \\ A_4^* &= \frac{-V^2}{2b\omega^2\eta_0} \int_{-1}^1 \tilde{C}_p x \sin \Psi_H dx = \frac{V^2}{2b\omega^2\eta_0} \int_{-1}^1 \tilde{C}_{pA_4^*} dx \end{aligned} \quad (3)$$

where, \tilde{C}_p =unsteady pressure amplitude reduced by dynamic pressure ($: 1/2\rho V^2$) per unit relative pitching angle induced by heaving or torsional motion, Ψ_H/Ψ_T =the phase-lag of the negative maximum of unsteady pressure from the maximum relative pitching angle for heaving/torsional

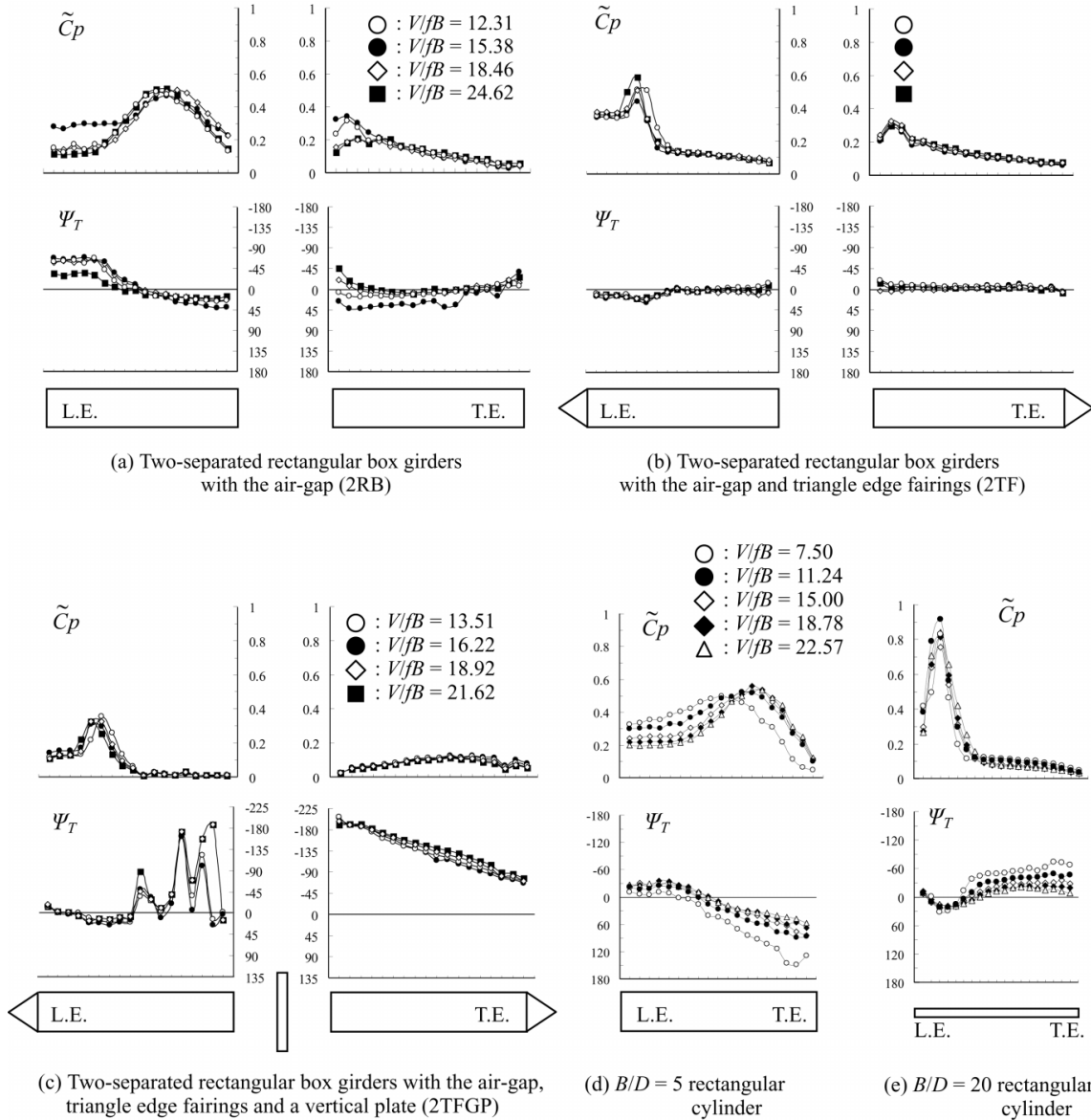
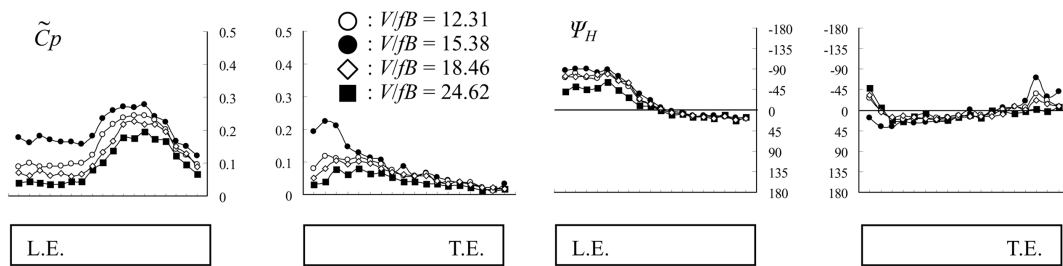


Fig. 2 The characteristics of unsteady pressure distribution in torsional 1DOF vibration of various structural sections

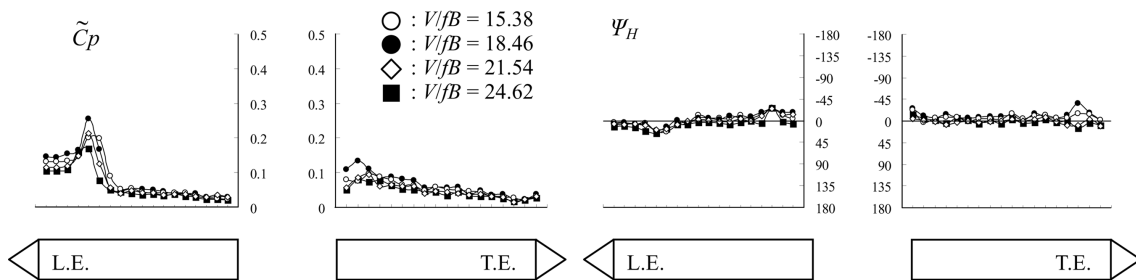
motion, η_0/φ_0 =amplitude of 1DOF heaving/torsional forced vibration. If the effect of the torsional velocity on the relative pitching angle can be neglected, the following relations are derived (Matsumoto, *et al.* 1996):

$$H_1^* = kH_3^*, H_4^* = -H_2^*, A_1^* = kA_3^* \text{ and } A_4^* = -kA_2^* \quad (4)$$

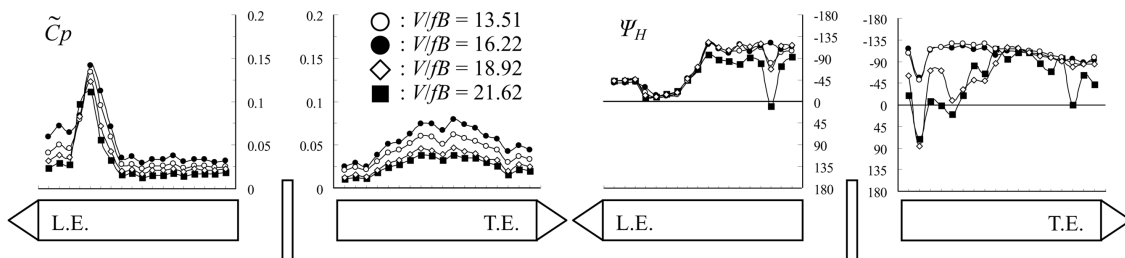
The fairly well dependence between the aerodynamic derivatives as shown in Eq. (4) is obtained for



(a) Two-separated rectangular box girders with the air-gap (2RB)



(b) Two-separated rectangular box girders with the air-gap and triangle edge fairings (2TF)



(c) Two-separated rectangular box girders with the air-gap, triangle edge fairings and a vertical plate (2TFGP)

Fig. 3 The diagrams of unsteady pressure distribution in heaving 1 DOF vibration of 2TFGP, two-separated rectangular box girders with the air-gap, triangle edge fairings and a vertical plate

various sections, such as a thin plate, 2D rectangular cylinders with various side-ratios B/D of 5 to 20, an isolated elliptical cylinder and so on (Matsumoto and Shijo 2001). The unsteady pressure properties, \tilde{C}_p and Ψ_T , of these three two-separated box girders in 1DOF torsional forced vibration are shown in Fig. 2 together with those of 2D rectangular cylinders with $B/D=5$ and 20. From these figures, the chord-wise distribution of \tilde{C}_p and Ψ_T of the upstream-side section of 2RB shows a similar feature with the ones of an isolated rectangular cylinder with the same side-ratio of 5. However, both \tilde{C}_p and Ψ_T of the down-stream side section of 2RB shows the complete different ones of 2RB or the up-stream-side section, because of the modified flow separation field in air-gap. On the other hand, those of the up-stream side section of 2TF are drastically influenced with the triangle edge fairing, but the ones of the downstream side section show the similar ones with the down-stream side section of 2RB. This means the less effect of the flow field around the up-stream side section on the down-stream side section. For 2TF, in particular, the phase of pressure, Ψ_T , are significantly reduced by triangle edge fairing. Furthermore, more drastic changes of \tilde{C}_p and Ψ_T of both up- and down-stream side sections are observed by installation of a gap-plate with 2D height at the air-gap part. It should be noted that a gap-plate should significantly affect on the flow fields not only of down-stream side section but also of the up-stream side one of 2TFGP during 1DOF torsional motion. Besides, similarity of the unsteady pressure properties, \tilde{C}_p and Ψ , in between 1DOF torsional forced vibration and 1DOF heaving one is observed for 2D rectangular cylinders with various side-ratios, 2RB, 2TF, and the other almost sections, but this similarity is not satisfied for 2TFGP (See those under 1DOF heaving forced vibration in Fig. 3). This would be explained by the bleeding effect by the torsional movement, in particular, the torsional velocity, of a gap-plate, and his bleeding effect can significantly change the flow field. As a matter of fact, disagreement of the unsteady pressure properties in between heaving and the torsional forced vibrations was

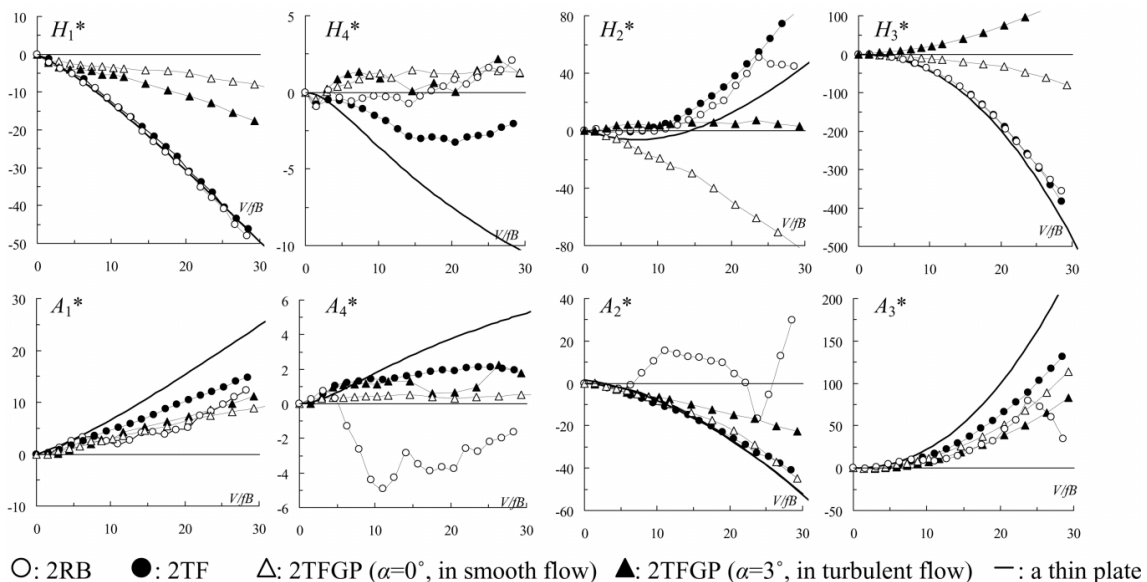


Fig. 4 The aerodynamic derivatives of two-separated rectangular girders with the air-gap

observed for the flat hexagonal box section with a vertical plate at the mid-chord point. Basing upon these the unsteady pressure measurement and the direct measurement of the unsteady lift and pitching moment under the heaving or the torsional forced vibration, eight aerodynamic derivatives of these three models, 2RB, 2TF and 2TFGP, are obtained as shown in Fig. 4 together with those of a thin plate obtained by Theodorsen function. Besides, Fig. 4 also shows the aerodynamic derivatives of 2TFGP under the condition of $\alpha=3^\circ$ and in turbulent flow (5%) compared with that under $\alpha=0^\circ$ and in smooth flow.

4. Flutter analysis and step-by-step method

The instability of flutter, which is divergent oscillation, is evaluated by its aerodynamic damping of each mode. Applying complex eigen-value analysis, both flutter circular frequency and aerodynamic damping are directly obtained. Complex eigen-value analysis is an exact solution, however the problem is that the contribution of the aerodynamic derivatives to the damping is not clear on data processing. On the other hand, SBSFA (Matsumoto, *et al.* 1994), developed by the authors based on the interaction between heaving and torsional motion through coupled terms of aerodynamic derivatives, could make it clear. In this method, logarithmic decrements of heaving branch δ_η , and torsional one δ_ϕ are expressed, respectively, as follows (Matsumoto, *et al.* 1994):

$$\delta_\eta = -\pi \left(\frac{\rho b^2}{m} \right) H_1^* - \pi \left(\frac{\rho b^2}{m} \right) \frac{\left(\frac{\rho b^4}{I} \right) \left(\frac{\omega_F}{\omega_\phi} \right)^2}{\sqrt{\left\{ 1 - \left(\frac{\omega_F}{\omega_\phi} \right)^2 \right\}^2 + 4 \zeta_\phi^2 \left(\frac{\omega_F}{\omega_\phi} \right)^2}} \times \{ |A_1^*| H_2^* \cos \theta_1 + |A_4^*| H_2^* \cos \theta_2 - |A_1^*| H_3^* \sin \theta_1 - |A_4^*| H_3^* \sin \theta_2 \} \quad (5)$$

where,

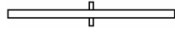
$$\begin{aligned} \omega_F &: \text{flutter circular frequency, } \omega_\phi: \text{torsional circular frequency, } \zeta_\phi: \text{torsional damping ratio,} \\ \theta &= \tan^{-1} (2 \zeta_\phi \omega_\phi \omega_\eta / \omega_\phi^2 - \omega_\eta^2) \\ \theta_1 &= \theta - \pi/2 \text{ for } A_1^* > 0, \quad \theta_1 = \theta + \pi/2 \text{ for } A_1^* < 0 \\ \theta_2 &= \theta \text{ for } A_4^* > 0, \quad \theta_2 = \theta + \pi/2 \text{ for } A_4^* < 0 \end{aligned}$$

$$\delta_\phi = -\pi \left(\frac{\rho b^4}{I} \right) A_2^* - \pi \left(\frac{\rho b^4}{I} \right) \frac{\left(\frac{\rho b^2}{m} \right) \left(\frac{\omega_F}{\omega_\eta} \right)^2}{\sqrt{\left\{ 1 - \left(\frac{\omega_F}{\omega_\eta} \right)^2 \right\}^2 + 4 \zeta_\eta^2 \left(\frac{\omega_F}{\omega_\eta} \right)^2}} \times \{ A_1^* |H_2^*| \cos \theta_1 + A_1^* |H_3^*| \cos \theta_2 - A_4^* |H_2^*| \sin \theta_1 - A_4^* |H_3^*| \sin \theta_2 \} \quad (6)$$

where,

$$\begin{aligned} \omega_\eta &: \text{heaving circular frequency, } \zeta_\eta: \text{heaving damping ratio, } \theta = \tan^{-1} (2 \zeta_\eta \omega_\eta \omega_\phi / \omega_\eta^2 - \omega_\phi^2) \\ \theta_1 &= \theta - \pi/2 \text{ for } H_2^* > 0, \quad \theta_1 = \theta + \pi/2 \text{ for } H_2^* < 0 \\ \theta_2 &= \theta \text{ for } H_3^* > 0, \quad \theta_2 = \theta + \pi/2 \text{ for } H_3^* < 0 \end{aligned}$$

Table 1 The aerodynamic and flutter characteristics of the well-stabilized structural sections against coupled flutter - flutter stabilization indices defined by $Vrcr/Vrcr_{plate}$, and the ratios of the important aerodynamic derivatives A_2^* , A_1^* and H_3^* to those of thin plate at reduced velocity $V/fB=20$

Geometrical shapes	Name	$Vrcr/Vrcr_{plate}$	$A_2^*/A_2^*_{plate}$	$A_1^*/A_1^*_{plate}$	$H_3^*/H_3^*_{plate}$	Remarks
	Modified rhombus	1.16	1.88	1.28	0.79	$(H_3^*$ control)
	Ellipse	1.01	0.75	0.52	1.59	A_1^* control
	Triangler	1.37	1.01	1.09	0.83	$(H_3^*$ control)
	$B/D=20$ rectangular with a vertical plate	1.11	3.75	2.05	0.79	$(H_3^*$ control)
	$B^*/D=5$ separated rectangular	0.56	(-0.18)	0.33	0.97	A_1^* control
	$B^*/D=5$ separated rectangular with a fairing	1.41	0.81	0.58	0.88	A_1^* control
	$B^*/D=5$ separated rectangular with fairing and a vertical plate	>1.9	0.92	0.52	0.16	A_1^* , H_3^* control

SBSFA method gives a fairly precise value in comparison with the complex eigen-value analysis. Especially, it is more useful for the clarification of the flutter instability mechanism because the aerodynamic damping for each branch can be explicitly expressed by the aerodynamic derivatives.

5. The role of aerodynamic derivatives on flutter instability

The SBSFA method gives the worthy information on the role of each aerodynamic derivative on the flutter instability for the torsional branch and the heaving one. For the torsional-branch coupled flutter, A_2^* , as stabilizing effect, and the combination of A_1^* and H_3^* , as destabilizing effect, play the

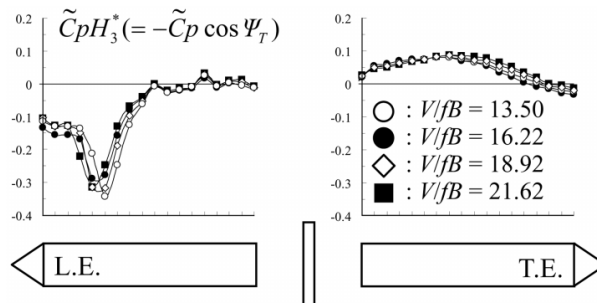


Fig. 5 $\tilde{C}_p H_3^*$ distribution diagram of 2TFGP, two-separated rectangular box girders with the air-gap, triangle edge fairings and a vertical plate

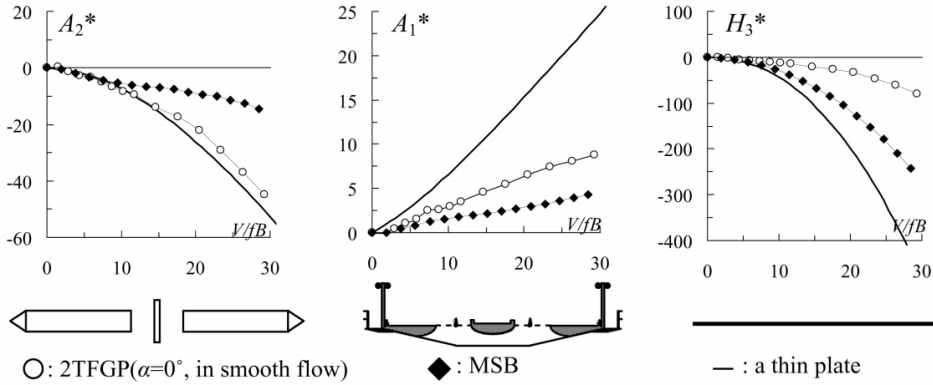


Fig. 6 The comparison of the aerodynamic derivatives A_2^* , A_1^* and H_3^* between 2TFGP (two-separated rectangular box girders with the air-gap, triangle edge fairings and a vertical plate) and MSB (Messina Strait Bridge)

definitely important role for the flutter instability, on the other hand, for the heaving-branch coupled flutter, H_1^* , as stabilizing effect, and the combination of A_1^* and H_3^* , as destabilizing effect, play also major role of flutter instability (Matsumoto, *et al.* 1994). Therefore, the reduction of the absolute value of A_1^* and H_3^* decreases the exciting coupling force, and then effectively stabilize the coupled flutter for both the torsional branch flutter and the heaving one. Table 1 shows the ratio of A_1^* and H_3^* at the reduced velocity of 20 to those of a thin plate for various bridges deck girders with more stability than a plate with the same structural dynamics, exceptionally 2RB section. From this table, therefore, the flutter stabilization can be classified into three different types of flutter stabilization, those are “ A_1^* -control” type, “ H_3^* -control” type and “ A_1^* and H_3^* -control” type. For three two-box girder sections, 2RB, 2TF and 2TRGP, former two sections are “ A_1^* -control” type and the last 2TRGP is “ A_1^* and H_3^* -control” type. As shown in Fig. 4, though three sections show A_1^* of similar values, H_3^* of 2TFGP can be significantly reduced than the other two. As shown in Fig. 5,

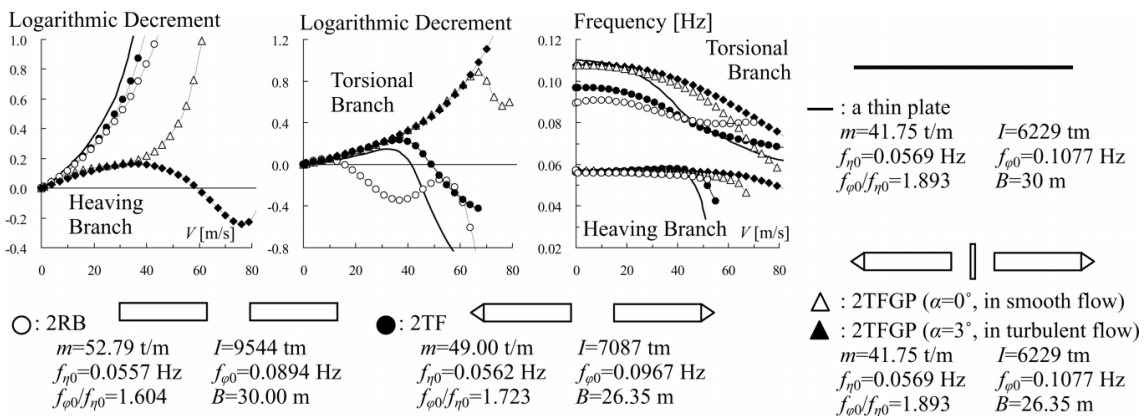


Fig. 7 $V-\delta$ and $V-f$ diagrams of various 2-separated box girders

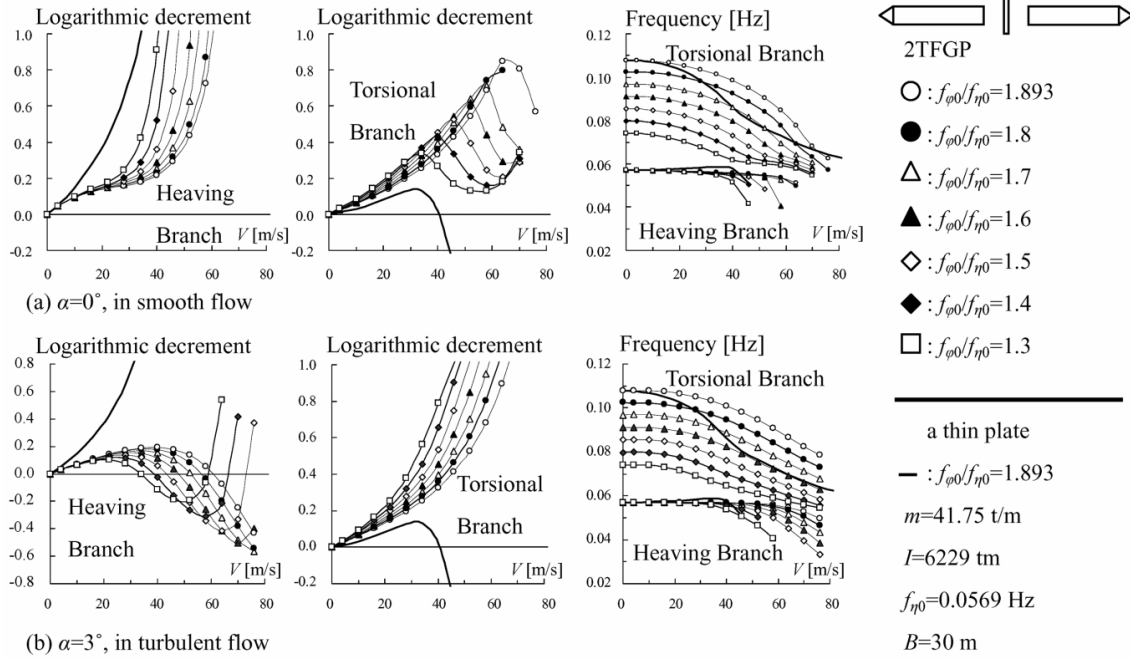


Fig. 8 Frequency ratio effects on flutter instability of 2TFGP, which are brought by changing natural frequency of torsional mode

which is $\tilde{C}_{pH_3^*} (= \tilde{C}_p \cos \Psi_T)$ chord-wise distribution diagram, the down-stream side section definitely contribute the H_3^* -reduction of 2TFGP section. From the point of the aerodynamic derivatives, 2TFGP section has better performance in the flutter stabilization than MSB girder, because of smaller absolute values of both A_2^* and H_3^* , in spite of a little bit larger A_1^* of 2TFGP than MSB girder as shown in Fig. 6. Using the structural dynamics of a virtual long suspension bridge with 3000 m main-span length, the $V-\delta$ diagram and $V-f$ diagram for the torsional and the heaving branch of these three two-box sections, obtained by the complex-eigen value analysis, are compared in Fig. 7. 2TFGP shows no flutter instability up to 80 m/s for the condition of $\alpha=0^\circ$ and in smooth flow, on the other hand, the heaving branch coupled flutter onsets approximately 60 m/s under $\alpha=3^\circ$ and in turbulent flow.

6. The effect of torsional/heaving frequency ratio on flutter characteristics

The flutter characteristics of structures are determined by not only the aerodynamic derivatives but also the structural dynamics. In particular, the torsional/heaving frequency ratio, $f_{\phi 0}/f_{\eta 0}$, of structures is a key parameter from the structural dynamic point, and the flutter critical reduced-velocity is almost proportional to it. It is well known that when the frequency, f_{ϕ} , of torsional branch approaches to or in particular case coincides with the one, f_{η} , of heaving branch, flutter instability begins. The frequency ratio of torsional and heaving branch, $f_{\phi 0}/f_{\eta 0}$, influences sensitively to the coupling forces at that situation, which can be understood as the effect on θ_1 . The examples of the frequency ratio effects on the $V-\delta$ diagrams and $V-f$ diagrams are shown in Fig. 8, respectively. As

shown in these figures, it is cleared that the flutter characteristics are rather sensitively and complicatedly influenced by the frequency ratio, $f_{\phi 0}/f_{\eta 0}$.

7. Conclusions

The conclusions obtained in this study are summarized as follows:

- (1) The two-separated box section with triangle faring at girder-edge and a vertical plate at a central air-gap (2TFGP) shows significantly good performance under the condition of angle of attack of 0° and in smooth flow against flutter instability by reducing the key-aerodynamic derivatives of A_1^* and H_3^* .
- (2) The significant reduction of H_3^* comes from the unsteady pressure characteristics of the down-stream section.
- (3) A vertical plate at a central air-gap generates the different unsteady pressure distribution under between heaving and torsional forced vibration, because of the “bleeding effect” from the plate edge due to torsional motion.
- (4) The different condition of angle of attack and flow alters the flutter property of 2TFGP from the torsional branch instability to heaving branch instability.
- (5) The torsional and heaving frequency ratio affects sensitively and complicatedly on the velocity-damping diagram due to direct influence on the coupling force near and after flutter appearance.

Finally, the authors would like to acknowledge to Ass. Prof. H. Shirato and research Ass. T. Yagi, of Kyoto University for their contribution to a series of wind tunnel tests.

References

- Matsumoto, M. *et al.* (1994), “On mechanism of flutter phenomena for structural sections”, *J. Struct. Eng.*, **42A**, 819-824.
- Matsumoto, M. *et al.* (1996), “Aerodynamic damping of prisms”, *J. Wind Eng. Ind. Aerodyn.*, **59**, 159-175.
- Matsumoto, M. *et al.* (1997), “Torsional flutter of bluff bodies”, *J. Wind Eng. Ind. Aerodyn.*, **69-71**, 871-882.
- Matsumoto, M. and Shijo, R. (2001), “Key point for flutter stabilization of long span bridge”, *Wind Hazard Mitigation in Urban Area*, TIP.
- Sato, H. *et al.* (2002), “Full aeroelastic model test of a super long-span bridge with slotted box girder”, *J. Wind Eng. Ind. Aerodyn.*, **90**(12-15), 2023-2032.
- Scanlan, R.H., Belbeau, J.G. and Budlong, K.S. (1974), “Indicial aerodynamic functions for bridge decks”, *J. Eng. Mech. Div., Proc. ASCE*, **100**(EM4), 657-672.